Nuclear Science and Techniques (2024) 35:72
https://doi.org/10.1007/s41365-024-01433-1

Neutron irradiation influence on high-power thyristor device under fusion environment

Wei Tong[1] · Hua Li[2] · Meng Xu[2,3] · Zhi-Quan Song[2] · Bo Chen[1]

Received: 26 September 2023 / Revised: 22 December 2023 / Accepted: 18 January 2024 / Published online: 9 May 2024

Abstract
Because of their economy and applicability, high-power thyristor devices are widely used in the power supply systems for large fusion devices. When high-dose neutrons produced by deuterium–tritium (D–T) fusion reactions are irradiated on a thyristor device for a long time, the electrical characteristics of the device change, which may eventually cause irreversible damage. In this study, with the thyristor switch of the commutation circuit in the quench protection system (QPS) of a fusion device as the study object, the relationship between the internal physical structure and external electrical parameters of the irradiated thyristor is established. Subsequently, a series of targeted thyristor physical simulations and neutron irradiation experiments are conducted to verify the accuracy of the theoretical analysis. In addition, the effect of irradiated thyristor electrical characteristic changes on the entire QPS is studied by accurate simulation, providing valuable guidelines for the maintenance and renovation of the QPS.

Keywords Fusion device · Neutron irradiation effects · Thyristor · Quench protection

1 Introduction

Tokamak is an experimental device used to develop nuclear fusion energy, in which the most easily achieved fusion reaction is the deuterium–tritium (D–T) fusion, which can be expressed as Eq. (1) [1, 2]. When the D–T fusion reaction occurs in a tokamak, approximately 80% of the energy is released in the form of 14.1 MeV fast neutrons [3–5]. Currently, the tokamak is in the experimental exploration stage, and certain windows and channels must be set up for observation, which may lead to an increase in the neutron irradiation flux in the fusion environment. Taking the ITER tokamak as an example [6], during a 500 MW D–T fusion reaction experiment, the number of fast neutrons produced by the plasma is 1.78×10^{20} n s^{-1} [7]. After installing the shielding layer and considering neutron attenuation, the calculated neutron flux rate in the entire host hall remains equal to 10^5 n cm^{-2} s^{-1}, which is far greater than the safety threshold and has a significant impact on the performance of the electrical devices around the tokamak [8, 9].

$$D + T \rightarrow n(14.1\,MeV) + {}^4He(3.5\,MeV) \quad (1)$$

A quench protection system (QPS) is typically designed to ensure the safety of the superconducting magnet in a tokamak [10, 11], in which thyristors are commonly used as the trigger units of the commutation circuit, as shown in Fig. 1 [12, 13]. QPS operates as follows: When a superconducting magnet is under normal operating conditions, the current flows through the bypass switch (BPS). Once the quench occurs, the BPS opens quickly, and the magnet current is transferred to the vacuum circuit breaker (VCB) via the arc voltage. Then, the thyristors turn on, owing to a pulse current generated by the charged capacitor *C* and

This work was supported by the Fundamental Research Funds for the Central University (No. JZ2023HGTA0182) and Comprehensive Research Facility for Fusion Technology Program of China (No. 2018-000052-73-01-001228).

✉ Hua Li
lihua@ipp.ac.cn

✉ Meng Xu
meng.xu@ipp.ac.cn

[1] School of Electrical Engineering and Automation, Hefei University of Technology, Hefei 230009, China

[2] Institute of Plasma Physics, Hefei Institutes of Physical Science, Chinese Academy of Sciences, Hefei 230031, China

[3] University of Science and Technology of China, Hefei 230026, China

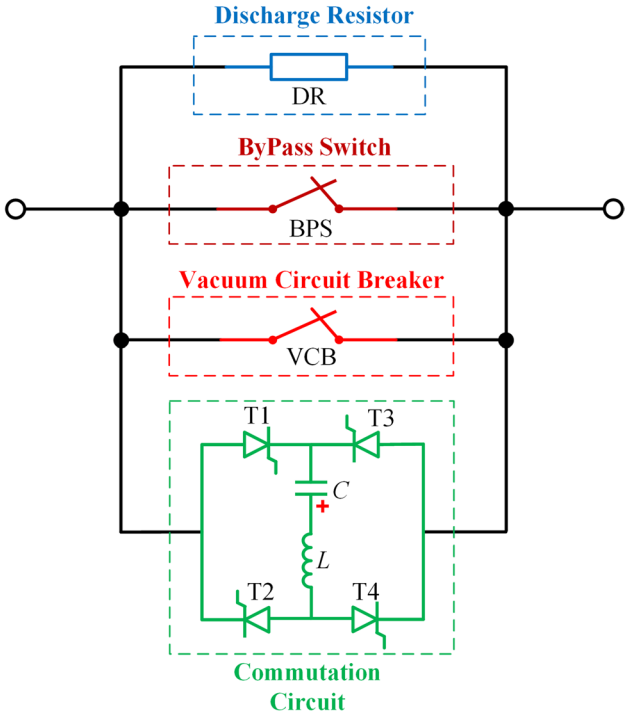

Fig. 1 (Color online) The circuit topology of QPS

pulsed inductor L, to reduce the current in the VCB to zero [14, 15]. Finally, the magnetic current is transferred to the discharge resistor (DR), and the energy stored in the magnet is constantly consumed until it reaches zero.

To protect the superconducting magnetic coils in the fusion device effectively, the QPS must respond as quickly as possible. To ensure that the QPS can accomplish this task, it should be located as close as possible to the magnetic coils, an area that unfortunately also exhibits a high fast neutron flux rate; thus, neutron damage cannot be avoided. The typical layout of the fusion device and irradiation nephogram are shown in Fig. 2 [8, 9]. If the thyristor switch is damaged by neutron irradiation and cannot operate normally, the current will not be interrupted sufficiently quickly by the VCB with the help of the auxiliary pulse current, which results in the failure of the QPS and destruction of the superconducting magnet [16].

Because the ITER device uses the D–T fusion route, neutron irradiation damage must be considered. Previous studies have focused on the main structural materials of fusion reactors, such as the first walls, blanket modules, and divertors [17–19]. Gradually, ITER acknowledged the threat of neutron irradiation to auxiliary equipment, and then conducted irradiation calculation, established exposure limits, and provided mitigation measures [8, 20, 21]. Researchers have conducted radiation reliability analysis based on the ITER guidelines, which is unfortunately insufficient, especially for high-power thyristors.

Semiconductor damage due to high- energy neutron irradiation is a topic of interest not only in the context of Tokamaks and Stellarators but also in the context of spacecrafts and satellites, where electronics are similarly bombarded with a complex mix of high-energy particles. [22–24]. Currently, in the literature, displacement damage and total ionization effects are observed in electronics, and few power devices have been studied separately at the macro and micro levels. However, because of the peculiarity of the fusion-neutron irradiation environment and requirement for effective irradiation reinforcement, the relationship between the internal physical structure and external electrical characteristic changes should be thoroughly studied.

Neutron irradiation damage and internal physical structure changes occurring on semiconductor devices have mainly been investigated experimentally. Yue et al. studied the synergistic effects of electrical stress and neutron irradiation on silicon carbide (SiC) power MOSFET devices. The defects in the devices were categorized using low-frequency noise (LFN) and deep-level transient spectrum (DLTS) methods [25]. Chen et al. conducted displacement damage dose (DDD) and total ionization dose (TID) irradiation experiments using a 14.1 MeV neutron high-voltage multiplier and 60Co gamma-rays to study the synergistic effect of TID and DDD on neutron-irradiated GaN HEMT [26]. However, the relationship between various physical parameters and electrical characteristics of semiconductor devices needs to be further investigated.

On the other hand, Ravotti and Mekki studied the I–V characteristic of PIN photodiodes under 1 MeV neutron irradiation at the European Organization for Nuclear Research (CERN) [27, 28]. Through numerous irradiation experiments and tests, the relationship curves of the forward conduction voltage drop and leakage current under different neutron fluxes were obtained. Liu et al. [29] experimentally studied the influence of fast neutron irradiation on the high di/dt switching characteristics of a pulse power supply insulated gate-triggered thyristor (IGTT). The corresponding simulation and test results indicated that neutron irradiation caused a significant decrease in the threshold and on-state voltages of IGTT. However, these studies did not provide a detailed description or exploration of the physical causes leading to changes in electrical characteristics.

In this study, we focused on the characteristic changes occurring in the thyristor switch within the QPS of a fusion device, as shown in Fig. 1. The internal physical structural changes of the thyristor caused by neutron irradiation were first introduced to obtain the possible physical parameters that may cause changes in the electrical characteristics. Then, considering the various key electrical parameters of thyristors, the relationship between the physical and electrical characteristics of thyristors after neutron irradiation was theoretically analyzed. Additionally, a series of

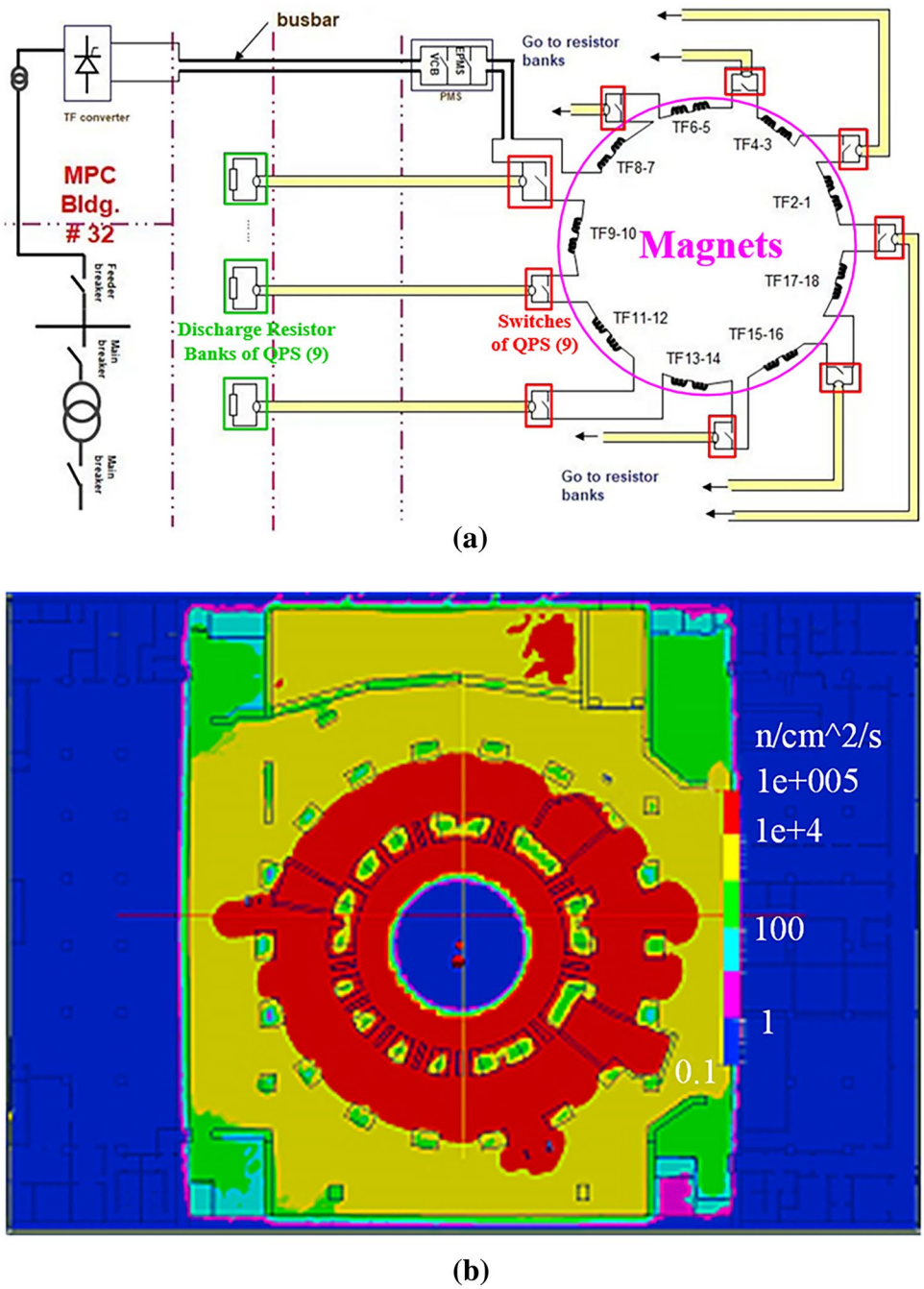

Fig. 2 (Color online) Typical layout of fusion device and irradiation nephogram. **a** Typical layout of fusion device. **b** Total neutron flux (TNF) caused by plasma in host hall; the max TNF is 10^5 n cm^{-2} s^{-1}

targeted thyristor physical simulations and neutron irradiation experiments were conducted to verify the accuracy of the theoretical analysis results. Furthermore, the effect of the irradiated thyristor characteristic changes on the entire QPS has been studied based on performance simulations. This study not only established a clear relationship between the changes occurring in the physical and electrical characteristics of the neutron-irradiated thyristor but also provided a valuable guideline for the maintenance and renovation of QPS.

2 Theoretical discussion of the relationship between physical and electrical characteristics changes in the thyristor after neutron irradiation

2.1 Damage mechanism analysis of the physical characteristics of thyristors after neutron irradiation

Because neutrons are electrically neutral and have a very strong penetrability, they can be sufficiently close to the atomic nucleus of the lattice atom of the material to be radiated and collide with the atomic nucleus elastically [30, 31]. The lattice atom receives energy during the collision, leaving its normal lattice position and becoming an interstitial atom in the lattice and leaving a vacancy in its original position. If vacancies and interstitial atoms remain within the Coulomb force field of the elastic force field, recombination can occur. If the force field is overcome, the interstitial atoms do not recover, causing an atomic displacement. The production processes of the vacancies and interstitial atoms are depicted in Fig. 3.

These vacancies can combine with adjacent atoms or other vacancies. Moreover, they can be moved to the vicinity of doping to form vacancy impurity complexes so that doping does not affect the conductivity, thus changing the density of doping. The displacement of a single atom forms a simple defect called the Frenkel Defect [32]. If the energy of the incident neutron is sufficiently high, the displaced interstitial atoms receive sufficient energy. The collision of such interstitial atoms displaces numerous atoms in the lattice, forming a large defect cluster.

The literature [33] indicates that when the incident neutron energy is 1 MeV, the average energy obtained by the initially displaced atom is 72.5 keV, whereas the displacement threshold for a Si atom is 15 eV. The D–T reaction produces a neutron energy of 14.1 MeV, which is approximately 1 million times the Si atomic shift threshold; thus, it has a significant impact on Si materials. In addition, a defect group generated by a 1 MeV neutron can include approximately 200 to 1000 displaced lattice atoms. Although the collision cross section between neutron and lattice atom is only between 10^{-23} cm^2 and 10^{-24} cm^2, the energy transferred to the lattice atom by collision is quite large; accordingly, a series of lattice atoms can eventually be displaced.

Semiconductor materials have three microscopic physical parameters: the minority carrier lifetime τ, pure doping density n, and mobility μ. Neutron irradiation introduces defects and defect clusters in the semiconductor, thus altering the three microscopic physical parameters and almost all parameters of the semiconductor device.

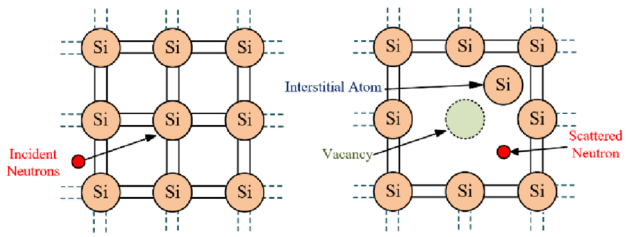

Fig. 3 (Color online) The production mechanism of vacancies and interstitial atoms in Si

Defects formed by neutron irradiation can introduce additional energy levels into the forbidden band of semiconductor materials, which increases the chance of recombination of minority and majority carriers, as well as the recombination rate, reducing the minority carrier lifetime. The relationship between the neutron flux and minority carrier lifetime is stated below.

$$\frac{1}{\tau(\phi)} = \frac{1}{\tau(0)} + k_\tau \times \phi, \tag{2}$$

where $\tau(0)$ and $\tau(\phi)$ denote the minority carrier lifetimes before and after neutron irradiation, respectively, k_τ denotes the minority carrier lifetime damage coefficient of the semiconductor materials, and ϕ denotes the neutron flux.

Because thyristors are semiconductor devices that use minority carriers as a conductive mechanism, minority carrier lifetime damage significantly affects the device performance.

In addition, neutron irradiation reduces the doping density of semiconductor materials, which is called the carrier removal effect. The relationship between the neutron flux and doping density is expressed below:

$$n(\phi) = n(0) - \frac{\Delta n}{\Delta \phi} \times \phi, \tag{3}$$

where $n(0)$ and $n(\phi)$ are the doping densities before and after neutron irradiation, respectively, $\Delta n/\Delta\phi$ is the carrier removal rate, and ϕ is the neutron flux.

In addition, when neutron irradiation introduces defects in the semiconductor materials, the defects can be used as scattering centers for carriers, effectively reducing the carrier mobility. The influence of the neutron irradiation on mobility can be expressed as follows:

$$\frac{1}{\mu(\phi)} = \frac{1}{\mu_{\mathrm{ID}}} + \frac{1}{\mu_{\mathrm{L}}} + \frac{A_{\mathrm{t}} \times \left[1 - \exp\left(\varepsilon_{\mathrm{T}} - \varepsilon_{\mathrm{f}}\right)/kT\right]}{B_{\mathrm{t}}}\phi, \tag{4}$$

where $\mu(\phi)$ is the mobility of carriers after neutron irradiation, μ_{ID} is the mobility due to stray atom scattering, μ_{L} is the mobility due to collision with thermal vibration lattice, A_{t} and B_{t} are coefficients, ε_{T} and ε_{f} are the defect and Fermi levels, respectively, k is Boltzmann constant, T is thermodynamic temperature, and ϕ is the neutron flux.

2.2 Establishing the relationship between physical and electrical characteristics change after neutron irradiation

As thyristors have longer lifetimes, higher reliability, less maintenance requirements, and higher rated power capability than other semiconductor devices, they have become the

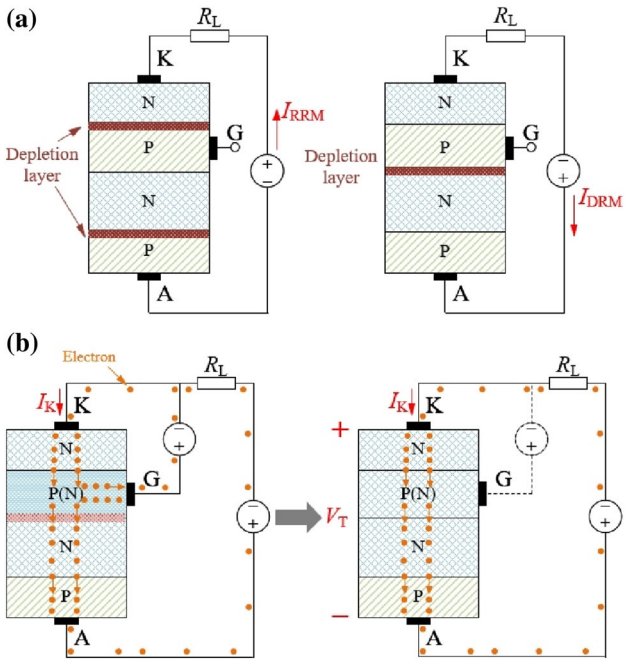

Fig. 4 (Color online) Internal structure diagram of a thyristor. **a** Blocking state. **b** Conducting state

first choice for QPS implementations in tokamak superconducting systems.

Thyristors consist of alternating P-type and N-type semiconductors (PNPN) [34]. As shown in Fig. 4, the depletion layer is formed at the junction of P-type and N-type semiconductor. If there is no external power supply to the gate of the thyristor, there will always be at least one reverse-biased depletion layer, regardless of the voltage direction of the external circuit, as shown in Fig. 4a. If the thyristor gate is supplied with an additional voltage, which is called a gate trigger, a large number of electrons will be injected into the P-region of the thyristor, which eventually becomes an N-region, causing the depletion layer width to gradually decrease and almost disappear, as shown in Fig. 4b. Because the injected electrons have already entered the N-region, even though the thyristor gate is not supplied with an additional voltage, it can still maintain its conducting state.

Therefore, both the blocking and conducting states of a thyristor after neutron irradiation can be analyzed by simplifying it as a PN diode.

2.2.1 Blocking characteristic

The blocking characteristic of a thyristor can be expressed as the reverse current of a PN junction under a reverse voltage, which can be divided into two conditions, as shown in Fig. 4a. Hence, the forward leakage current I_{DRM} and reverse leakage current I_{RRM} are the two most crucial parameters for evaluating the blocking characteristic of thyristors. Figure 5

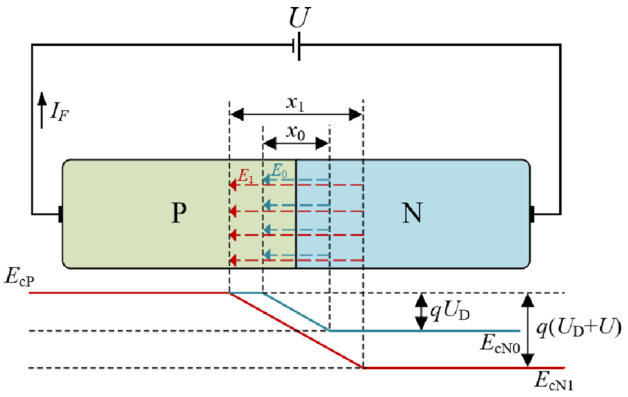

Fig. 5 (Color online) The change in the PN junction barrier region under reverse bias

depicts the change in the PN junction barrier region under reverse bias. When the applied electric field E is in the same direction as the self-built electric field E_0, the electric field in the depletion layer is enhanced. The enhancement of the electric field causes the barrier region to widen as well as increase in height.

Meanwhile, the balance between the diffusion and drift of carriers is broken owing to the growth of the barrier region, in which drift plays a dominant role. Therefore, the electrons at the boundary of the P-region can be pulled to the N-region, and the holes at the boundary of the N-region can be pulled to the P-region. Meanwhile, the electrons in the P-region and holes in the N-region drift toward the boundary to supplement and form the reverse current I_F, which is directed from the N-region to P-region, as shown in Fig. 6. However, because there are few electrons in the P-region and few holes in the N-region, the reverse current I_F is minimal.

If the recombination of electrons and holes in the barrier region is neglected, the current density J through the PN junction can be considered as the sum of the hole diffusion current density $J_p(x_N)$ passing through the x_N and electron diffusion current density $J_n(x_P)$ passing through the x_P [34].

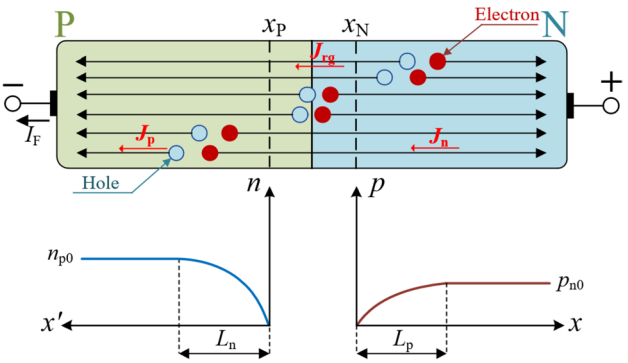

Fig. 6 (Color online) The diagram of reverse current generation and minority distribution

$$J = J_p(x_N) + J_n(x_P), \tag{5}$$

$J_p(x_N)$ can be calculated using the following equations if the hole and electron density distributions are known:

$$J_p(x_N) = -qD_p \frac{d\Delta p_n(x)}{dx}\bigg|_{x=x_N}, \tag{6}$$

where $d\Delta p/dx$ is the hole density gradient and D_p is the hole diffusion coefficient.

If the P- and N-regions are sufficiently long, the non-equilibrium carrier concentration in the PN junction should be distributed exponentially.

$$\Delta p_n(x) = \left[p_n(x_N) - p_{n0}\right] \exp\left(\frac{x_N - x}{L_p}\right), \tag{7}$$

where L_p is the hole-diffusion length.

$$L_p = \sqrt{D_p \tau_p} \tag{8}$$

Moreover,

$$p_n(x_N) = p_{n0} \exp\left(\frac{qU}{kT}\right), \tag{9}$$

where p_{n0} is the equilibrium minority carrier concentration in the N-region and U is the applied reverse voltage. Therefore, $J_p(x_N)$ is calculated as follows:

$$J_p(x_N) = \frac{qD_p p_{n0}}{L_p}\left[\exp\left(\frac{qU}{kT}\right) - 1\right]. \tag{10}$$

Analogously,

$$J_n(x_P) = \frac{qD_n n_{p0}}{L_n}\left[\exp\left(\frac{qU}{kT}\right) - 1\right]. \tag{11}$$

Consequently,

$$J = \left(\frac{qD_n n_{p0}}{L_n} + \frac{qD_p p_{n0}}{L_p}\right)\left[\exp\left(\frac{qU}{kT}\right) - 1\right], \tag{12}$$

$$I_F = AJ = A\left(\frac{qD_n n_{p0}}{L_n} + \frac{qD_p p_{n0}}{L_p}\right)\left[\exp\left(\frac{qU}{kT}\right) - 1\right], \tag{13}$$

where A is the cross-sectional area of the PN junction. As U approaches negative infinity, $\exp(qU/kT)$ approaches zero.

$$I_F = -A\left(\frac{qD_n n_{p0}}{L_n} + \frac{qD_p p_{n0}}{L_p}\right) = -I_0. \tag{14}$$

Therefore, I_F increases as the carrier lifetime τ_p and τ_n is greatly shortened after neutron irradiation. In addition, for a silicon PN junction, the recombination current density J_{rg} in barrier region significantly affects the reverse current. After neutron irradiation, the number of recombination centers in the barrier region of the PN junction increases, and the carrier generation rate increases, which leads to an increase in the recombination current.

As a result, after neutron irradiation, the reverse current I_F in PN junction increases, increasing both the forward leakage current I_{DRM} and reverse leakage current I_{RRM} of the irradiated thyristor.

2.2.2 Conducting characteristic

The conduction characteristics of a semiconductor can be characterized by its on-state resistance or on-state voltage drop U_{TM}. The lower the U_{TM}, the better the high-current performance of the device; this is a significant parameter of the semiconductor that is used in QPS of the fusion device, given the extremely high current-breaking requirements of the superconducting magnet.

To achieve high working voltage capability, the substrate resistivity of the PN junction diode should generally be high, that is, the substrate doping concentration should be low with a wide substrate region. Therefore, the defects caused by neutron irradiation lead to a carrier removal effect in the semiconductor material, resulting in numerous conductive carrier constraints and inhibiting conduction. Thus, the resistivity increases, which increases the conducting voltage of PN junction.

Based on the abovementioned analysis, the conducting characteristics of a thyristor can be analyzed by simplifying it as a PN diode. The on-state voltage drop of a PN diode U_{TM} can be divided into two parts: one is the junction voltage U_j formed by the internal electric field, and the other is the voltage related to the substrate epitaxial layer U_b. Note that U_j is minimal and negligible.

$$U_T = U_j + U_b \approx U_b, \tag{15}$$

According to the literature [33], U_b can be expressed as follows:

$$U_b = \frac{Iw_d}{A\sigma_p}, \tag{16}$$

where w_d is the base region width of PN junction and σ_p is the conductivity of the P-region.

The conductivity of the irradiated material can be derived as follows:

$$\sigma(\phi) = \sigma(0)e^{-\alpha\phi}, \tag{17}$$

$$\ln\frac{\sigma(0)}{\sigma(\phi)} = \alpha\phi. \tag{18}$$

When ϕ approaches 0, the following equation holds:

$$\alpha = \frac{1}{\sigma(0)} \times \left.\frac{\mathrm{d}\sigma(\phi)}{\mathrm{d}\phi}\right|_{\phi\to 0}. \tag{19}$$

Accordingly,

$$\sigma = q\mu p, \tag{20}$$

where μ is the majority carrier mobility of PN diode and p is the base doping concentration of PN diode.

Subsequently,

$$R = \left.\frac{\mathrm{d}p}{\mathrm{d}\phi}\right|_{\phi\to 0}, \tag{21}$$

$$\alpha = \frac{q\mu(\phi)}{\sigma(0)} \times R, \tag{22}$$

$$\ln\frac{\sigma(0)}{\sigma(\phi)} = \frac{q\mu(\phi)}{\sigma(0)} \times R\phi, \tag{23}$$

where R is the carrier removal rate.

According to Eq. (16)

$$\sigma = \frac{Iw_\mathrm{d}}{AU_\mathrm{b}}. \tag{24}$$

Substituting Eq. (24) into Eq. (23), the following expression is obtained:

$$\frac{U_\mathrm{b}(\phi)}{U_\mathrm{b}(0)} = \exp\left[\frac{q\mu(\phi)}{\sigma(0)} \times R\phi\right] > 1. \tag{25}$$

From the abovementioned analysis, it can be concluded that U_b increases because of the majority carrier removal effect in the PN junction. In addition, the change in the irradiated thyristor on-state voltage drop U_TM is determined based on the irradiation intensity, which is discussed through further neutron irradiation simulations and experiments.

2.2.3 Reverse recovery characteristic

Reverse recovery is also called "turning off" a thyristor after it reaches a conducting state; the time required for the switch from conducting to blocking state is critical and needs to be minimized. Typically, neutron damage decreases the reverse recovery time because the minority carrier lifetime of the thyristor is significantly shortened after irradiation.

The typical reverse recovery current waveform is shown in Fig. 7. I_P is the peak value of the forward current. $t_\mathrm{s} = t_2 - t_1$ is the time required for the reverse current to increase from zero to its maximum value I_RM, which is called the storage time. $t_\mathrm{f} = t_3 - t_2$ is the time required for the current to decrease from I_RM to $0.1I_\mathrm{RM}$, which is called the fall time. The total reverse recovery time is denoted as $t_\mathrm{rr} = t_\mathrm{s} - t_\mathrm{f}$, where Q_rr is the reverse recovery charge [35].

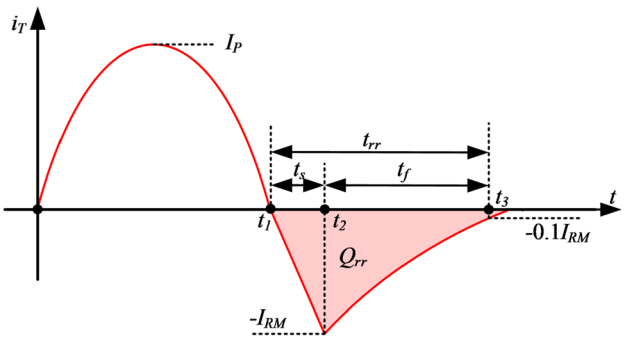

Fig. 7 (Color online) The typical reverse recovery current waveform

When the thyristor is in the conducting state, most of the charge is stored in the base region, which is formed by minority carriers. The charge continuity equation is stated as follows:

$$i_\mathrm{T}(t) = \frac{\mathrm{d}Q}{\mathrm{d}t} + \frac{Q}{\tau}, \tag{26}$$

where $i_\mathrm{T}(t)$ is the current flowing through the thyristor, Q is the charge stored in the base region, and τ is the minority-carrier lifetime.

The thyristors in QPS correspond to the trigger unit of the commutation circuit, which is composed of a pulsed inductor L and charged capacitor C. To simplify the analysis, the forward conducting current is considered to be sinusoidal, such that $i_\mathrm{T}(t) = I_\mathrm{P}\sin wt$. According to Eq. (26), the following expression can be obtained:

$$Q(t) = \frac{K_0 I_\mathrm{P}\tau}{1 + w^2\tau^2}\left(w\tau e^{-t/\tau} + \sin wt - w\tau\cos wt\right), \tag{27}$$

where K_0 is the current gain of the thyristor.

At t_1, charge $Q(t_1)$ can be calculated using Eq. (27)

$$Q(t_1) = \frac{K_0 I_\mathrm{P} w\tau^2}{1 + w^2\tau^2}\left(1 + e^{-\pi/w\tau}\right). \tag{28}$$

When the forward current drops to zero, a large number of non-equilibrium carriers that remain in the thyristor are dissipated by sweeping out and recombination. At time t_2, the current reaches I_RM, and the thyristor begins to recover its reverse blocking capability. At this time, only a small amount of the stored charge remains in the base region. These charges disappear via recombination, which is called the low-injection condition. However, high-power semiconductor devices generally operate under large-injection conditions; therefore, it can be assumed that $Q(t_2) = 0$. According to Eq. (27), the following expression is obtained:

$$\sin wt_2 = w\tau\left(\cos wt_2 - e^{-t_2/\tau}\right). \tag{29}$$

As $t_2 = t_1 + t_s = \pi/w + t_s$, $wt_2 = \pi + wt_s$. In addition, wt_s is far less than $\pi/2$; thus, wt_s is considered to be approximately zero. Then, observe that $\sin wt_s \approx wt_s$ and $\cos wt_s \approx 1$. Therefore,

$$\sin wt_2 = \sin\left(\pi + wt_s\right) = -\sin\left(wt_s\right) \approx -wt_s, \tag{30}$$

$$\cos wt_2 = \cos\left(\pi + wt_s\right) = -\cos\left(wt_s\right) \approx -1. \tag{31}$$

Approximating Eq. (29), the expression for t_2 is stated as follows:

$$t_s \approx \tau\left(1 + e^{-t_2/\tau}\right), \tag{32}$$

t_2 is much longer than τ. Therefore,

$$t_s \approx \tau. \tag{33}$$

Then, the maximum reverse current I_{RM} can be expressed as follows:

$$I_{RM} \approx k\left(t_2 - t_1\right) = k\tau, \tag{34}$$

where k is the forward current change rate at t_1.

Based on the abovementioned analysis, it can be concluded that after high-dose neutron irradiation of the thyristor, which reduces the minority carrier lifetime τ, the reverse recovery characteristics undergo significant changes. According to Eq. (33) and Eq. (34), the storage time t_s and maximum reverse current I_{RM} decrease with a reduction in τ, which means that the total turn-off time of the semiconductor t_{rr} is reduced as a result of high-dose neutron irradiation. In addition, the reverse recovery charge Q_{rr} decreases sharply after irradiation.

3 Neutron irradiation simulation

To verify the accuracy of the abovementioned theoretical analysis regarding the thyristor damage mechanism under fusion-neutron irradiation, qualitative verification through material- and device-level simulations based on a simplified thyristor model must be conducted. The idea behind the simulation implemented in this study is that after neutron irradiation, the device material lattice is damaged, and the defects introduce additional energy levels, which affect the electrical characteristics of the device. Therefore, two types of defects are mainly considered in this study: donor defects characterized by $E_C - 0.12$ eV, and acceptor defects characterized by $E_V + 0.21$ eV.

APSYS, an advanced semiconductor device physical model simulation software, is used for the simulations conducted in this study. A thyristor is an extremely complex device and its design is often patented and proprietary. Therefore, such designs are regarded as commercial secrets. Therefore, a general and widely used physical model of a thyristor is established to simulate the effect of neutron irradiation on the electrical characteristics of thyristor devices. Accordingly, the 2D model of the device and doping concentration considered in this study are shown in Fig. 8.

Mathematical models primarily include basic and key models. The basic model includes the drift diffusion model, Poisson equation, continuity equation, and ohmic contact electrical boundary. The key model includes the mobility, collision ionization, and bulk defect models. After determining the physical parameters of the thyristor model, the basic

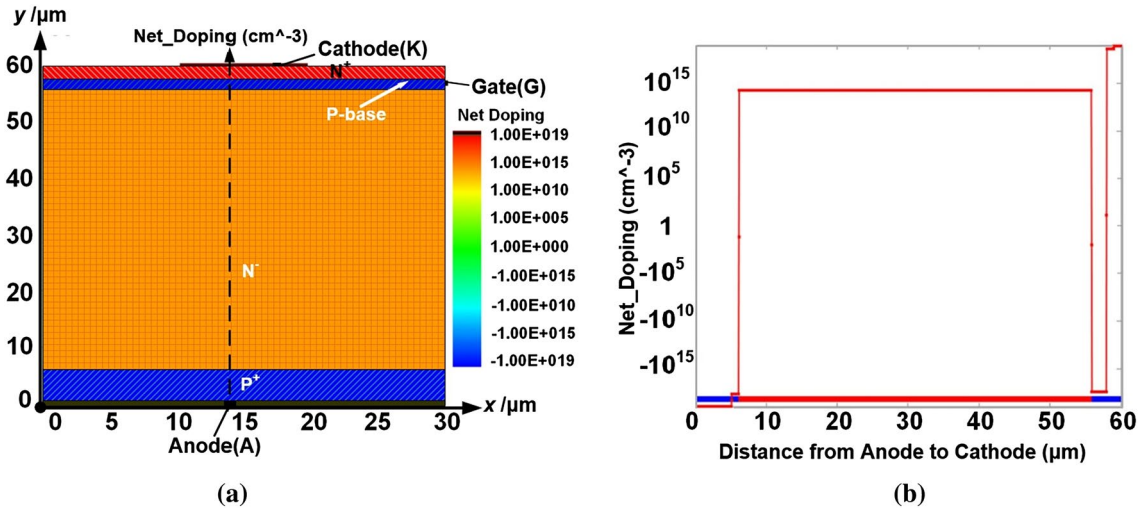

Fig. 8 (Color online) Simulation model of the thyristor. **a** 2D model. **b** doping concentration

semiconductor equations are solved numerically by combining the initial and boundary conditions, and the electrical parameters under a specific bias voltage are obtained.

The blocking characteristics of the thyristor are presented in Fig. 9a. Observe that the leakage current of the thyristor increases sharply when the reverse voltage is 350 V. When $U_{AK} = -400$ V, according to the 2D electric field distribution shown in Fig. 9b, the main electric field is in the N-region.

The on-state characteristics of the thyristor are presented in Fig. 10. Observe that when the triggering voltage $V_G = 0.5$ V, the thyristor is not triggered, whereas when $V_G = 1$–5 V, the thyristor is triggered.

The blocking characteristics of thyristor before and after the neutron irradiation are shown in Figs. 11 and 12, respectively, for comparison. When the thyristor is subjected to the same voltage, the forward and reserve leakage currents I_{DRM} and I_{RRM} increase under both donor and acceptor defect effects.

The on-state characteristics of thyristors before and after neutron irradiation are shown in Figs. 13 and 14, respectively, for comparison. Observe that when the thyristor is supplied with the same current, the on-state voltage drop U_{TM} increases after irradiation under both donor defect and acceptor defect effects.

The simulation results show that the forward and reverse leakage currents and on-state voltage of thyristor increase after neutron irradiation, which is consistent with the theoretical analysis presented earlier.

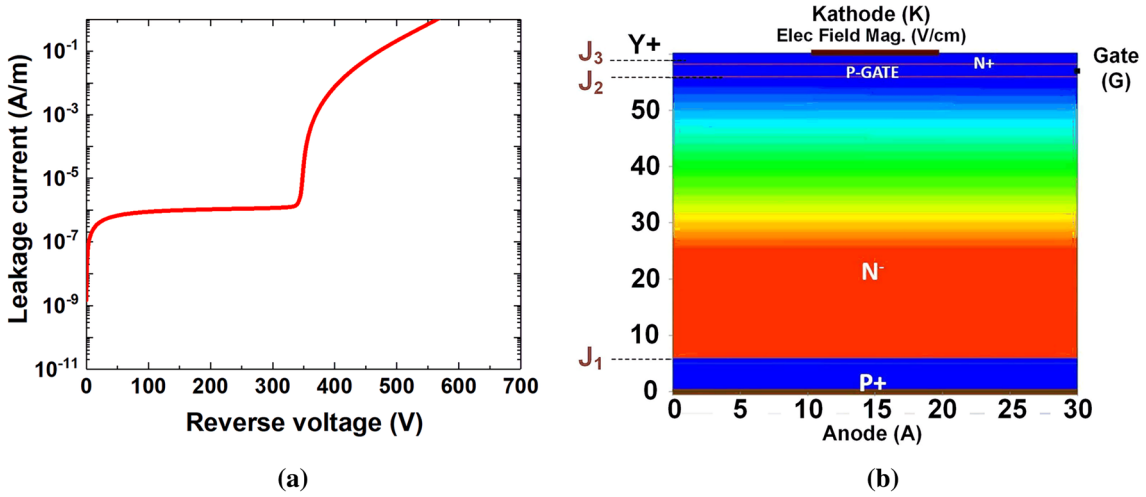

Fig. 9 (Color online) Blocking characteristic. **a** *I*–*V* characteristic. **b** 2-D electric field distribution ($U_{AK} = -400$ V)

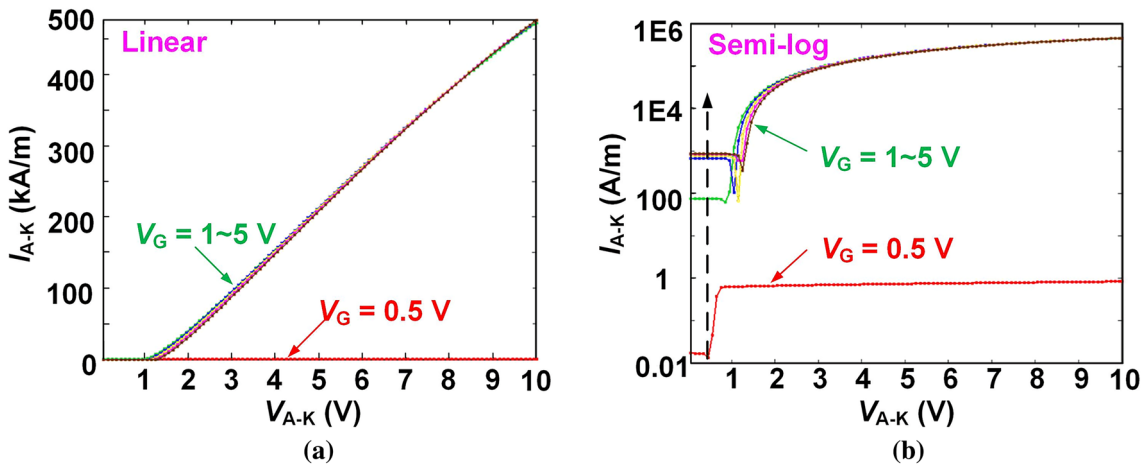

Fig. 10 (Color online) Conducting characteristic. **a** Linear. **b** Semi-log

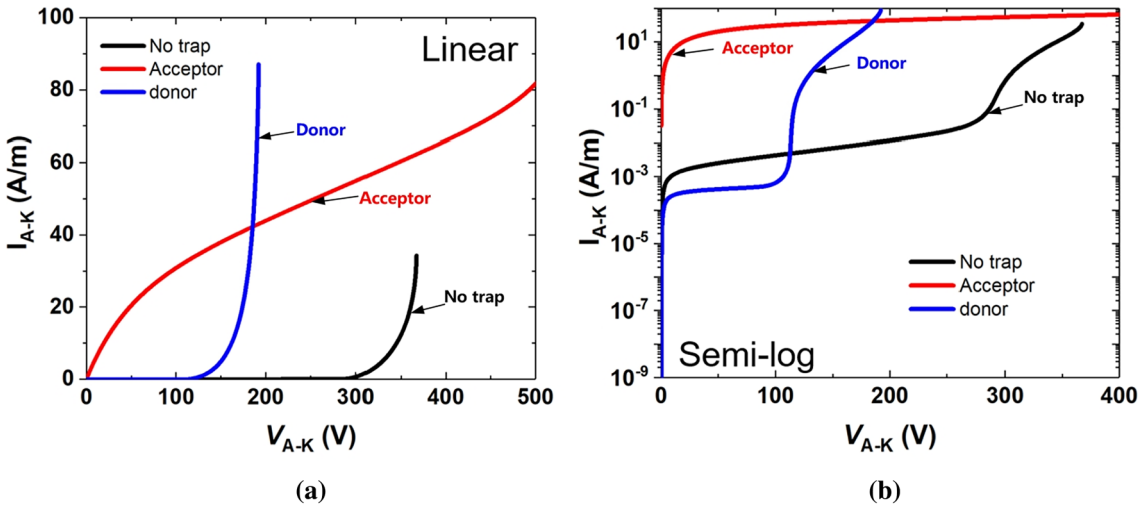

Fig. 11 (Color online) I_{DRM} of irradiated thyristor (donor-type and acceptor-type defect). **a** Linear. **b** Semi-log

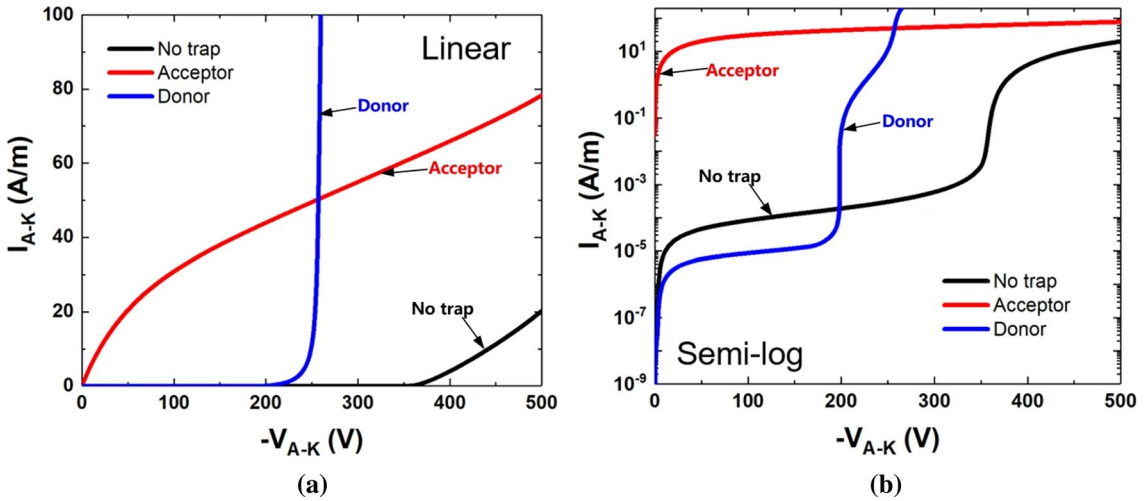

Fig. 12 (Color online) I_{RRM} of irradiated thyristor (donor-type and acceptor-type defect). **a** Linear. **b** Semi-log

4 Neutron irradiation experiment

This study uses a D–T neutron generator for irradiation, which is based on an accelerator neutron source affiliated with the China Academy of Engineering Physics (CAEP), Mianyang, China. The experiment is conducted on a K-400 accelerator, using an accelerated deuterium (D) beam to irradiate the tritium (T) target to achieve the D–T reaction, producing fast neutrons with an energy of approximately 14.1 MeV.

To improve the efficiency of the neutron irradiation experiment, a new device layout mode, called the stepped layout mode is proposed, as shown in Fig. 15. Six ABB 5STP 52U5200 thyristor devices are distributed in three spherical spaces with different irradiation radii, in which two thyristors in each radius face the neutron source with the anode and cathode.

According to the neutron calculation report published by ITER, the neutron flux rate at QPS can be as high as 10^5 n cm^{-2} s^{-1} with local shielding. In this study, the average neutron flux rate is considered to be 10^4 n cm^{-2} s^{-1}. Assuming that the duty cycle of ITER operation is 0.5, the annual operating time is estimated as 1.58×10^7 s; therefore, the neutron flux at QPS can reach 1.58×10^{11} n cm^{-2}. To obtain more extreme results, the neutron flux 20 cm away from the neutron source is set to 4.3×10^{11} n cm^{-2}, which is 2.7 times larger than the actual irradiation environment. Subsequently, the output number of the neutron source can be calculated using the following formula:

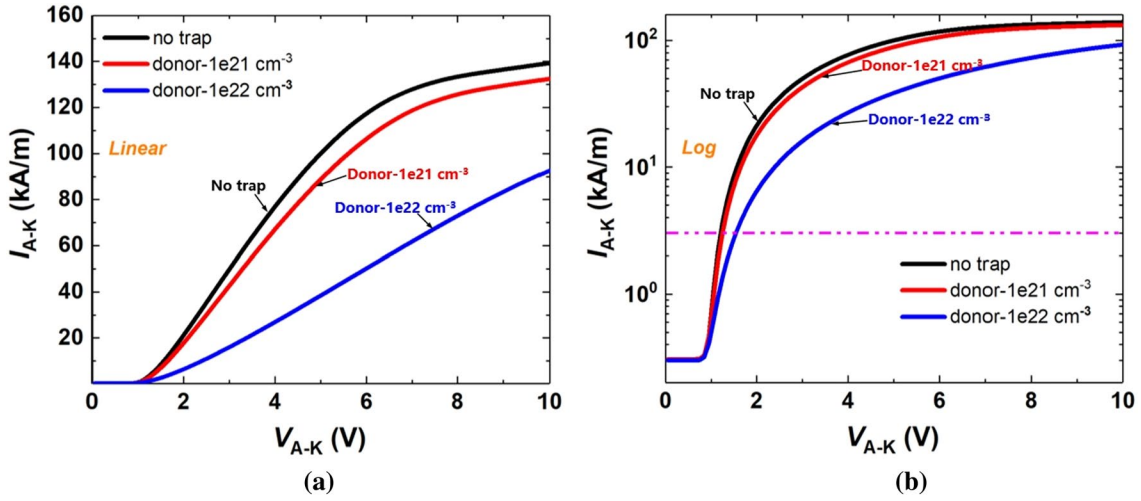

Fig. 13 (Color online) U_{TM} of irradiated thyristor (donor-type defect). **a** Linear. **b** Semi-log

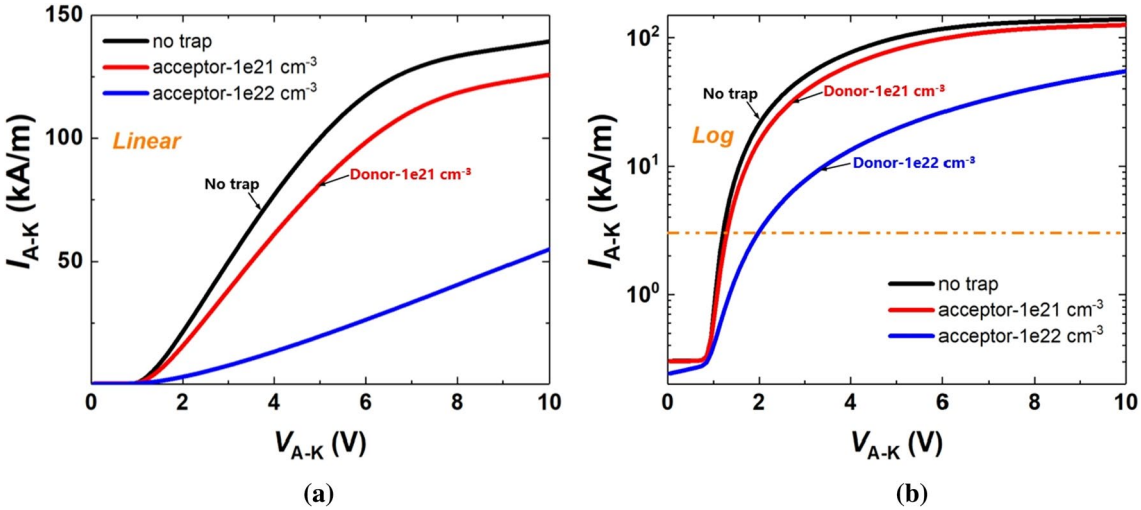

Fig. 14 (Color online) U_{TM} of irradiated thyristor (acceptor-type defect). **a** Linear. **b** Semi-log

$$n_{\text{Total}} = \phi \times 4\pi r^2 = 2.16 \times 10^{15} \text{ n}. \tag{35}$$

During the irradiation experiment, the cumulative irradiation time is 95,373 s, and the final number of neutrons produced by the D–T neutron generator is 2.55×10^{15} n (uncertainty of 4%), which meets the experimental requirements.

In addition, the neutron fluxes of the devices from near to far are 1:1/4:1/9, and the cross-sectional area of the irradiated thyristor is 233 cm^2. Therefore, the neutron flux and neutron injection number of the thyristors at each position can be calculated.

The thyristor stack in QPS is used as the trigger unit of the commutation circuit, which is shown in Fig. 1, the temperature of the thyristor is not obvious after being supplied with a 1 ms/100 kA pulse current. Therefore, the electrical parameters that need to be tested when the device temperature is 25°C are considered as the key testing data. The tested thyristor number and location are reported in Table 1.

The changes in each thyristor parameter before and after neutron irradiation are shown in Fig. 16. Observe that the tested electrical parameters of the thyristors exhibit significant changes after neutron irradiation. As the thyristors are placed 20 cm, 40 cm, and 60 cm away from the neutron source, the corresponding neutron fluxes received by the thyristors could be calculated as 4.3×10^{11} n cm^{-2}, 1.07×10^{11} n cm^{-2}, and 0.48×10^{11} n cm^{-2}, respectively. The forward and reverse leakage currents, namely, I_{DRM} and I_{RRM}, respectively, represent the blocking characteristics of the thyristor. I_{DRM} increases to 637 μA, 528 μA, and 452.5 μA, respectively, and I_{RRM} increases to 615.5 μA,

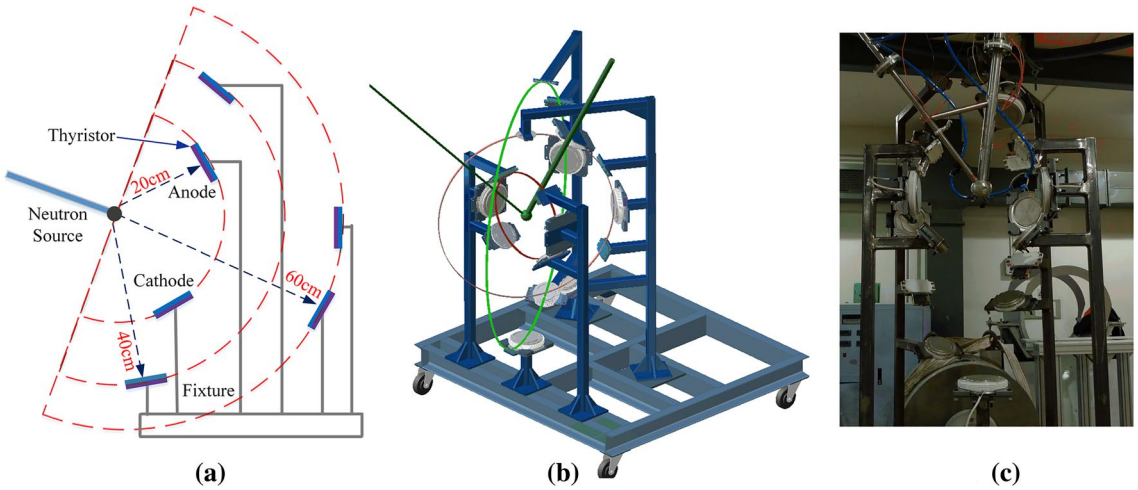

Fig. 15 (Color online) Schematic diagram of neutron irradiation experiment. **a** 2D space distribution. **b** 3D space distribution. **c** Neutron source

Table 1 The thyristor number and location in 14.1 MeV neutron irradiation experiment

Location (cm)	20	40	60
Neutron flux (n cm^{-2})	4.3×10^{11}	1.07×10^{11}	0.48×10^{11}
Number	#1#2	#3 #4	#5 #6

458 μA, and 422.5 μA, respectively. The on-state voltage drop U_{TM} of the irradiated thyristors at different distances from the neutron source increases from 1.26 to 4.325 V, 1.84 V, and 1.415 V, respectively. In addition, the values of Q_{rr} and t_{rr} are significantly reduced after neutron irradiation, as shown in Figs. 16d and e, which indicates that the severity of the reverse recovery process is reduced and duration is shortened after neutron irradiation.

In terms of the impact degree, the blocking characteristics and reverse recovery characteristics of the irradiated thyristor are seriously affected; a hundred-fold change is observed in their key parameters. Meanwhile, the conducting performance of the most severely irradiated thyristors decreased by approximately 3/4, as indicated by the increase in the on-state voltage drop U_{TM}. The following conclusions can be drawn from Fig. 16, the higher the irradiation flux received by the thyristor is, the greater are the impact on the thyristor electrical parameters and performance damage to the thyristor.

5 Simulation analysis of the influence of neutron irradiation on QPS

QPS is a crucial system for not only superconducting magnets but also fusion devices. However, it is impractical and risky to conduct irradiation experiments on actual systems. With the development of simulation technology and PLECS software, the simulation accuracy has been significantly improved, which can effectively simulate the real QPS electrical performance under normal and operating states. Hence, simulation methods are used to study the effect of neutron irradiation on QPS.

The high-dose neutron irradiation on the thyristor stack may cause a huge risk of QPS breakdown in fusion devices. Therefore, it is important to analyze the impact of neutron irradiation on QPS. Because irradiation experiments conducted on QPS are risky and unfeasible, a prediction simulation method is adopted in this study. A simplified QPS circuit in the PLECS software and typical working current waveform are shown in Fig. 17 [36].

According to the irradiation experiment results, both the static parameters, namely, I_{DRM}, I_{RRM}, and U_{TM}, and dynamic parameters, namely, Q_{rr} and t_{rr}, change significantly after irradiation and may cause the QPS to fail.

The thyristor stack is turned off and maintained in the blocking state when QPS in at steady state, in which the capacitor in the commutation circuit is charged to a preset voltage. Therefore, an increase in I_{DRM} may cause a decrease in the capacitor voltage. Once the capacitor voltage decreases to a certain value, the pulse current generated by the commutation circuit cannot force the current in VCB down to zero, resulting in QPS failure. The larger the I_{DRM} is, the shorter is the time required for the capacitor voltage to drop to the threshold. The breaking failure waveform is shown in Fig. 18. The capacitor does not remain in the reverse-blocking state; therefore, I_{RRM} has almost no obvious impact on QPS.

The thyristor stack is turned on and on-state condition is maintained only when the commutation circuit generates a reverse pulse current. Therefore, a change in U_{TM} affects the characteristics of the pulse current, as shown in Fig. 19.

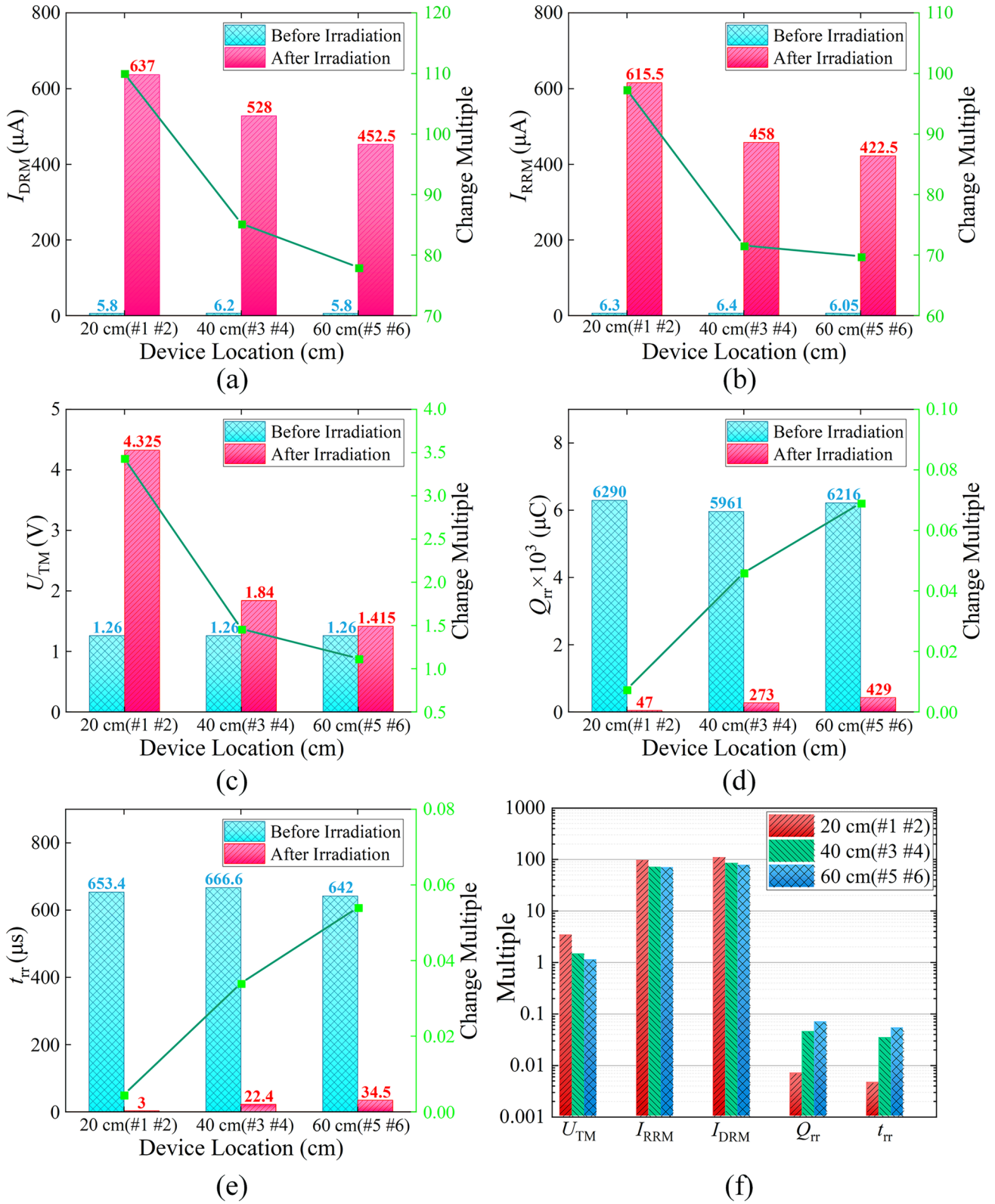

Fig. 16 (Color online) The change in each thyristor parameter before and after neutron irradiation. **a** Change in I_{DRM}. **b** Change in I_{RRM}. **c** Change in U_{TM}. **d** Change in Q_{rr}. **e** Change in t_{rr}. **f** Change ratio

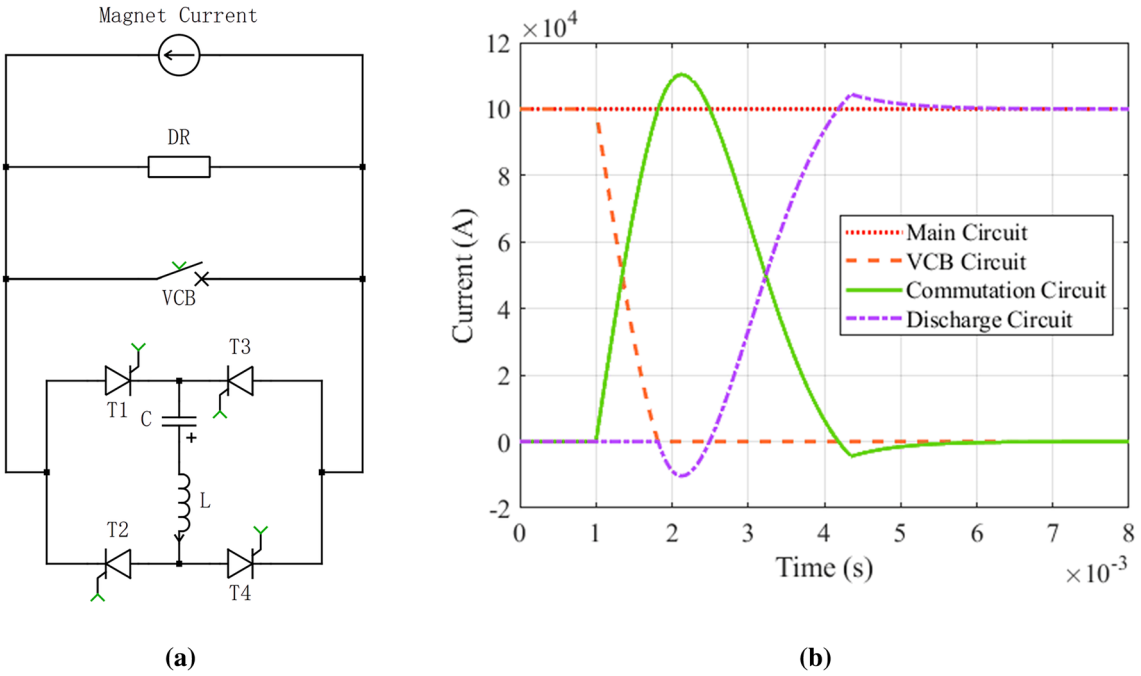

Fig. 17 (Color online) **a** Simplified simulation circuit. **b** Typical current waveform of QPS

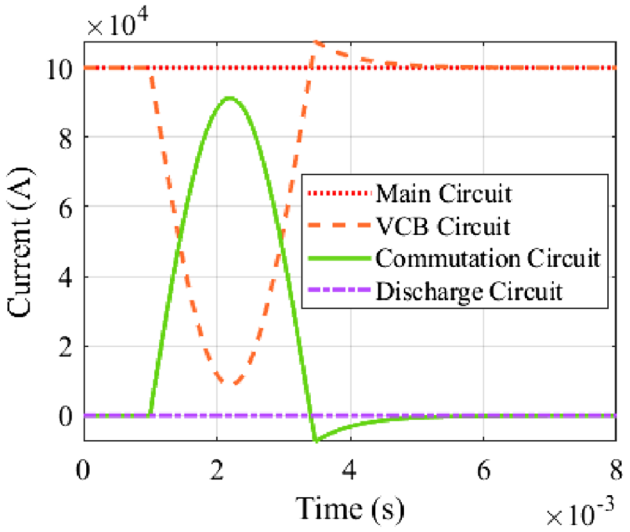

Fig. 18 (Color online) Breaking failure waveform of VCB

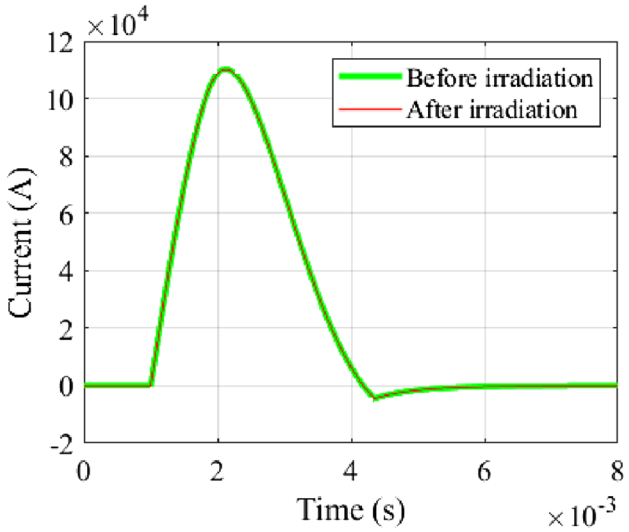

Fig. 19 (Color online) Comparison of the influence of U_{TM} change on the reverse pulse current of QPS

Observe that the pulse currents before and after irradiation are almost the same, which suggests that the impact of U_{TM} change on QPS is relatively minor.

Theoretical analysis and experimental verification reveal that the reverse-recovery characteristics of the thyristor change significantly. Q_{rr} and t_{rr} decrease after irradiation, indicating that the reverse recovery speed of the irradiated thyristor is accelerated. In QPS, multiple thyristor devices are connected in series to improve the voltage withstanding capability. Because each thyristor receives different neutron irradiation doses, the change ratios of the reverse recovery speeds differ. The voltage waveforms of the series-connected thyristors are shown in Fig. 20. Observe that before neutron irradiation, the series voltage sharing effect of the four thyristors is sufficient. In contrast, after neutron irradiation, a higher recovery voltage is applied to the thyristor which yields a faster reverse recovery speed. This unexpected event

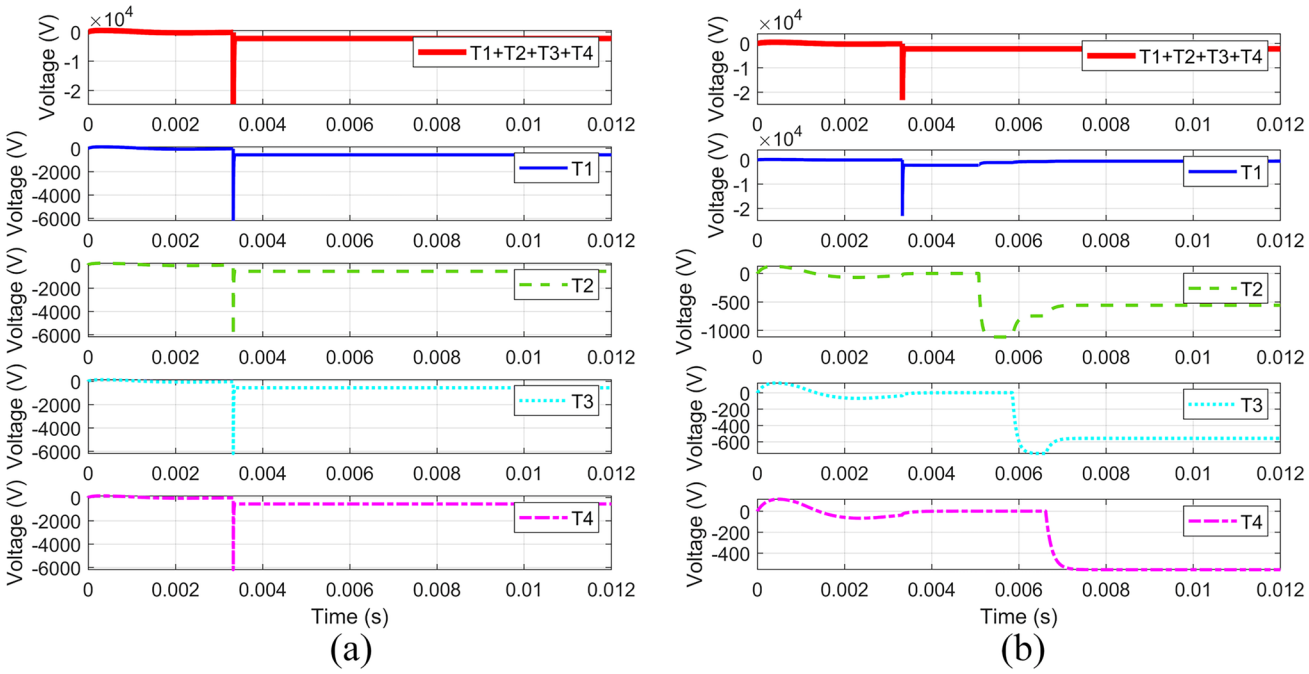

Fig. 20 (Color online) The voltage waveform of the thyristors during the reverse recovery process before and after neutron irradiation. **a** Before neutron irradiation. **b** After neutron radiation

damages the device owing to overvoltage, leading to damaging the entire thyristor stack and ultimately resulting in the failure of QPS quench current interruption and transfer actions.

6 Summary

This study investigates the influence of neutron irradiation on high-power thyristor devices under a fusion environment. By establishing the relationship between the internal physical structure and external electrical parameters of the thyristor, the effect of neutron irradiation on the thyristor is comprehensively analyzed. To verify the accuracy of the theoretical analysis, a series of targeted thyristor physical simulations and neutron irradiation experiments are conducted. The simulation and experimental results indicate that the dynamic and static characteristics of the irradiated thyristors change significantly, which is consistent with the theoretical analysis results. In addition, the effect of irradiated thyristors change on QPS used in the fusion device is simulated using the PLECS software. The simulation results show that the U_{TM} change has little impact on QPS, and the increase in I_{DRM} may lead to VCB breaking failure as the preset voltage of the capacitor in the commutation circuit decreases. The inconsistent reverse recovery speed of the irradiated thyristors leads to a high reverse voltage in the device, which may cause a breakdown and reduce the reliability and stability of the QPS. In future fusion devices, neutrons should be confined to the main engine, which could significantly mitigate the irradiation problem. In future research, the safe operational limits for thyristors under irradiation environments will be studied in depth to further ensure the reliability of the operating thyristors in QPS of Tokamak fusion devices, including irradiation-sensitive area localization, changing relationship between neutron flux and key electrical parameters, and degradation thresholds of these parameters.

Author contributions All authors contributed to the study conception and design. Material preparation, data collection and analysis were performed by Wei Tong, Meng Xu, Hua Li, Zhi-Quan Song and Bo Chen. The first draft of the manuscript was written by Wei Tong and all authors commented on previous versions of the manuscript. All authors read and approved the final manuscript.

Data availability The data that support the findings of this study are openly available in Science Data Bank at https://cstr.cn/31253.11.sciencedb.j00186.00409 and https://www.doi.org/10.57760/sciencedb.j00186.00409.

Declarations

Conflict of interest The authors declare that they have no Conflict of interest.

References

1. K. Tomabechi, J.R. Gilleland, Y.A. Sokolov et al., ITER conceptual design. Nucl. Fusion **31**, 1135 (1991). https://doi.org/10.1088/0029-5515/31/6/011
2. J. Li, Y. Wan, The experimental advanced superconducting tokamak. Engineering **7**, 1523–1528 (2021). https://doi.org/10.1016/j.eng.2021.10.004
3. J. Ongena, R. Koch, R. Wolf, H. Zohm, Magnetic-confinement fusion. Nat. Phys. **12**, 398–410 (2016). https://doi.org/10.1038/nphys3745
4. M. Yiğit, E. Tel, Theoretical determination of (d, n) and (d, 2n) excitation functions of some structural fusion materials irradiated by deuterons. Nucl. Sci. Tech. **28**, 245–253 (2017). https://doi.org/10.1007/s41365-017-0316-6
5. W. Chen, L. Hu, G. Zhong et al., Study on the gamma rays and neutrons energy response optimization of a scintillating fiber detector for EAST with Geant4. Nucl. Sci. Tech. **34**, 134 (2023). https://doi.org/10.1007/s41365-023-01290-4
6. W. Zhou, X. Fang, J. Fang et al., DC performance and AC loss of cable-in-conduit conductors for International Thermonuclear Experimental Reactor. Nucl. Sci. Tech. **27**, 74 (2016). https://doi.org/10.1007/s41365-016-0061-2
7. S. Zheng, M. Chen, J. Li et al., Neutronics analysis for the test blanket modules proposed for EAST and ITER. Nucl. Fusion **47**, 1053–1056 (2008). https://doi.org/10.1088/0029-5515/47/8/040
8. D. Martin et al., NIU report on radiation issues on electronics in B11. ITER Org., Marseille, Tech. Rep. (2016)
9. W. Tong, M. Xu, H. Li et al., The effects of neutron irradiation on the electrical characteristics of high-power thyristor, in *2023 IEEE 6th International Electrical and Energy Conference (CIEEC)* (2023), pp. 2362–2365. https://doi.org/10.1109/ICET55676.2022.9825404
10. W. Tong, M. Xu, H. Li et al., The conceptual design of upgraded 100 kA quench protection system for CRAFT superconducting magnet. Fusion Eng. Des. **187**, 113397 (2022). https://doi.org/10.1016/j.fusengdes.2022.113397
11. W. Zhou, X. Fang, J. Fang et al., Numerical and experimental analysis of AC loss for CFETR CS model coil. Nucl. Sci. Tech. **28**, 142 (2017). https://doi.org/10.1016/j.fusengdes.2022.113397
12. M. Xu, W. Tong, H. Li et al., Research on dynamic voltage balancing of series connected thyristors in auxiliary oscillation zero-crossing circuit. IEEE Trans. Plasma Sci. **51**, 164–171 (2023). https://doi.org/10.1109/TPS.2022.3231596
13. M. Xu, H. Li, Z. Song et al., The challenge and solution of overvoltage for 100 kA quench protection system in CRAFT project. Fusion Eng. Des. **175**, 113001 (2022). https://doi.org/10.1016/j.fusengdes.2022.113001
14. W. Tong, M. Xu, H. Li et al., 100 kA/10 kV thyristor stack design for quench protection system in CRAFT. Plasma Sci. Technol. **25**, 055601 (2023). https://doi.org/10.1088/2058-6272/aca8eb
15. W. Tong, Z. Song, P. Fu et al., Feasibility analysis of 100 kA DC commutation scheme to be applied in the quench protection unit of CFETR. IEEE Trans. Appl. Supercon. **30**, 1–9 (2020). https://doi.org/10.1109/TASC.2019.2926376
16. H. Li, Z. Song, S. Wang et al., Study on DC protection switch for superconducting coils in magnetic confinement fusion device. Proc. CSEE **36**, 233–239 (2016). https://doi.org/10.13334/j.0258-8013.pcsee.161406
17. C.R. Nobs, J. Naish, L.W. Packer et al., Computational evaluation of N-16 measurements for a 14 MeV neutron irradiation of an ITER first wall component with water circuit. Fusion Eng. Des. **159**, 111743 (2020). https://doi.org/10.1016/j.fusengdes.2020.111743
18. H.L. Swami, M. Abhangi, S. Sharma et al., A neutronic experiment to support the design of an Indian TBM shield module for ITER. Plasma Sci. Technol. **21**, 065601 (2019). https://doi.org/10.1088/2058-6272/ab079a
19. C. Yin, D. Terentyev, S. Van Dyck et al., Effect of high-temperature neutron irradiation on fracture toughness of ITER-specification tungsten. Phys. Scr. **2020**, 014052 (2020). https://doi.org/10.1088/2058-6272/ab079a
20. Overview of the ITER policy on electronics exposed to radiation
21. Overview of the implementing procedure of the ITER policy on electronics exposed to radiation
22. J. Prinzie, F.M. Simanjuntak, P. Leroux et al., Low-power electronic technologies for harsh radiation environments. Nat. Electron. **4**, 243–253 (2021). https://doi.org/10.1038/s41928-021-00562-4
23. D. Li, C. Li, M. Xiao et al., Deconstructing plasma fog collection technology: an experimental study on factors impacting collection efficiency. J. Phys. D Appl. Phys. **75**, 075201 (2024). https://doi.org/10.1088/1361-6463/ad0ac2
24. G. Liu, X. Wang, M. Li et al., Effects of high-energy proton irradiation on separate absorption and multiplication GaN avalanche photodiode. Nucl. Sci. Tech. **29**, 139 (2018). https://doi.org/10.1007/s41365-018-0480-3
25. S. Yue, Z. Chen, Z. Zhang et al., Synergistic effect of electrical stress and neutron irradiation on silicon carbide power MOSFETs. IEEE Trans. Electron. Dev. **69**, 3341–3346 (2022). https://doi.org/10.1109/TED.2022.3170539
26. R. Chen, Y. Liang, J. Han et al., Research on the synergistic effect of total ionization and displacement dose in GaN HEMT using neutron and gamma-ray irradiation. Nanomaterials **12**, 2126 (2022). https://doi.org/10.3390/nano12132126
27. F. Ravotti, M. Glaser, M. Moll et al., BPW34 commercial p-i-n diodes for high-level 1-MeV neutron equivalent fluence monitoring. IEEE Trans. Nucl. Sci. **55**, 2133–2140 (2008). https://doi.org/10.1109/TNS.2008.2000765
28. J. Mekki, M. Moll, M. Fahrer et al., Prediction of the response of the commercial BPW34FS silicon p-i-n diode used as radiation monitoring sensors up to very high fluences. IEEE Trans. Nucl. Sci. **57**, 2066–2073 (2010). https://doi.org/10.1109/TNS.2010.2044191
29. C. Liu, C. Yang, W. Chen et al., Experimentally demonstrating fast neutron irradiation effect on high-di/dt switching characteristics of insulated gate triggered thyristor for pulse power, in *2022 IEEE 34th International Symposium on Power Semiconductor Devices and ICs (ISPSD)* (2022), 177–180. https://doi.org/10.1109/ISPSD49238.2022.9813637
30. S.J. Watts, J. Matheson, I.H. Hopkins-Bond et al., A new model for generation-recombination in silicon depletion regions after neutron irradiation. IEEE Trans. Nucl. Sci. **43**, 2587–2594 (1996). https://doi.org/10.1109/23.556840
31. U. Biggeri, E. Borchi, M. Bruzzi et al., Comparison of radiation damage in silicon detectors induced by pions, protons and neutrons. Il Nuovo Cimento A **1965–1970**(109), 1351–1358 (1996). https://doi.org/10.1007/BF02773521
32. T.K. Maiti, C.K. Maiti, Modeling of radiation-induced displacement damage in silicon solar cells: Frenkel defect, in *2009 16th IEEE International Symposium on the Physical and Failure Analysis of Integrated Circuits* (2009), pp. 647–649. https://doi.org/10.1109/IPFA.2009.5232562
33. P. Chen, *Radiation Effects on Semiconductor Devices and Integrated Circuits* (National Defense Industry Press, Beijing, 2005)
34. E. Liu, B. Zhu, J. Luo, *The Physics of Semiconductors*, 7th edn. (Publishing House of Electronics Industry, Beijing, 2017)
35. W. Tong, H. Li, P. Fu et al., Parameter optimization of thyristor snubber circuit in LSTF quench protection system. IEEE Access

7, 81257–81265 (2019). https://doi.org/10.1109/ACCESS.2019.2923442

36. P. Górecki, D. Wojciechowski, Accurate computation of IGBT junction temperature in PLECS. IEEE Tran. Electron Dev. **67**, 2865–2871 (2020). https://ieeexplore.ieee.org/document/9093206